Nanoscale

PAPER

View Article Online
View Journal | View Issue

Cite this: *Nanoscale*, 2015, **7**, 16054

B_{11}^-: a moving subnanoscale tank tread†

Ying-Jin Wang,[a,b] Xiao-Yun Zhao,[a] Qiang Chen,[a] Hua-Jin Zhai*[a,c] and Si-Dian Li*[a]

Received 6th June 2015,
Accepted 22nd August 2015

DOI: 10.1039/c5nr03732h

www.rsc.org/nanoscale

We present a concept that an elongated, planar boron cluster can serve as a "tank tread" at the sub-nanometer scale, a novel propulsion system for potential nanomachines. Density functional calculations at the PBE0/6-311+G* level for the global-minimum B_{11}^- C_{2v} ($^1A_1$) and B_{11} C_{2v} ($^2B_2$) structures along the soft in-plane rotational mode allow the identification of their corresponding B_{11}^- C_{2v} and B_{11} C_{2v} transition states, with small rotational energy barriers of 0.42 and 0.55 kcal mol^{-1}, respectively. The energy barriers are refined to 0.35 and 0.60 kcal mol^{-1} at the single-point CCSD(T) level, suggesting that the clusters are structurally fluxional at room temperature. Molecular dynamics simulations show that B_{11}^- and B_{11} behave exactly like a tank tread, in which the peripheral B_9 ring rotates almost freely around the B_2 core. A full turn of rotation may be accomplished in around 2 ps. In contrast to molecular wheels or Wankel motors, the peripheral boron atoms in the tank tread behave as a flexible chain gliding around, rather than as a rigid wheel rotation. This finding is beyond imagination, which expands the concepts of molecular wheels and Wankel motors.

1. Introduction

In nanoscience and nanotechnologies, the nanovehicles and relevant nanomachines are fascinating subjects of pursuit.[1] It has remained an issue of debate whether there are fundamental problems in building a nanomachine that has every atom in its intended place, or whether "magic fingers" exist at all to accomplish such tasks.[2,3] However, this debate does not hold back the explorations along this direction. Pushing the miniaturization to the limit, one reaches the 1 nm or even sub-nanometer scale, where nanoclusters serve as mechanical parts. Boron clusters have clear advantages for this purpose due to their unique planar or quasi-planar geometries over a wide size range (B_n^- and B_n; n up to 40),[4–9] which are unprecedented for an element in the periodic table, facilitating the fabrication of free-standing, atomic-layer-thick nanoscale objects.

Notably, all-boron molecular wheels B_8^{2-} and B_9^- and a concentric dual π aromatic B_{19}^- cluster were observed lately,[10,11] the latter motivating the immediate proposal of a fluxional molecular Wankel motor.[12,13] Other molecular Wankel motors (B_{13}^+ and B_{18}^{2-}) were also studied computationally.[14–16] These molecular wheels and Wankel motors possess circular shapes. Structural fluxionality in three-dimensional Si clusters[17] was also discussed.

Depending on the size, boron clusters also adopt less circular, elongated structures. However, the dynamic fluxionality of such boron clusters has not been studied, probably because the inner core in an elongated cluster may be intuitively considered as a bar that halts the intramolecular motions. Here we report on an exploratory study along this direction. We show computationally that, contrary to anticipation, the elongated boron clusters B_{11}^- and B_{11} are structurally fluxional, which are analogous to a continuous track, or a "tank tread". In contrast to molecular wheels or Wankel motors, the peripheral boron atoms in B_{11}^- and B_{11} tank treads behave as a flexible chain gliding around, not as a rigid wheel. A full turn of the tank tread rotation may be accomplished in about 2 ps. The dimension of the tank treads is roughly 0.5 nm, being probably the smallest one can imagine of. This finding shall open the door to the invention and discovery of a variety of relevant nanostructures. We stress explicitly that the current subnanoscale tank treads are purely a proof-of-concept. At the current stage we are not intended to claim them as real nanoscale objects in the nanoworld, although such B_{11}^- and B_{11}

[a]*Nanocluster Laboratory, Institute of Molecular Science, Shanxi University, Taiyuan 030006, China. E-mail: hj.zhai@sxu.edu.cn, lisidian@sxu.edu.cn*
[b]*Department of Chemistry, Xinzhou Teachers University, Xinzhou 034000, China*
[c]*State Key Laboratory of Quantum Optics and Quantum Optics Devices, Shanxi University, Taiyuan 030006, China*

†Electronic supplementary information (ESI) available: A short movie extracted from the molecular dynamics (MD) simulation for B_{11}^-; optimized structures of the C_{2v} ($^1A_1$) global minimum (GM) and C_{2v} ($^1A_1$) transition state (TS) of B_{11}^- and those of their corresponding B_{11} neutral clusters at the PBE0/6-311+G* level; the total electron localization function (ELF) of the GM of B_{11}^- C_{2v} ($^1A_1$); chemical bonding in the C_{2v} TS of B_{11}^- as revealed from the ELF and adaptive natural density partitioning (AdNDP) analyses; the structural evolution of B_{11} during the peripheral rotation; and the Cartesian coordinates for the GM structures of B_{11}^- C_{2v} ($^1A_1$), B_{11} C_{2v} ($^2B_2$), and their C_{2v} TS states at the PBE0/6-311+G* level. See DOI: 10.1039/c5nr03732h

clusters are readily producible in the gas-phase experiments[18,19] without the needs of aid from the "magic fingers".

2. Methods

The global-minimum (GM) structures of B_{11}^- and B_{11} were constructed based on the literature[18–22] and fully reoptimized at the PBE0/6-311+G* level.[23,24] The QST2 calculations as implemented in the Gaussian 09 program[25] were carried out to search their in-plane rotational transition states (TS). Intrinsic reaction coordinate (IRC) calculations were performed to confirm that the TS is truly associated with the GM. For an accurate evaluation of the rotational energy barrier, further calculations were carried out at the single-point CCSD(T)/6-311G*//PBE0/6-311+G* level.[26] The Born–Oppenheimer molecular dynamics (BOMD) simulations were performed at the PBE0/6-31G level, at the temperatures of 300, 600, and 900 K. Chemical bonding analyses were performed using the canonical molecular orbitals (CMOs), electron localization function (ELF),[27] and adaptive natural density partitioning (AdNDP)[21,28] and visualized using the Molekel program.[29] All calculations were accomplished using the Gaussian 09 package,[25] except for the AdNDP analyses.[21]

3. Results and discussion

3.1. Molecular dynamics

The GM structures, B_{11}^- C_{2v} ($^1A_1$) and B_{11} C_{2v} ($^2B_2$), are well established in the literature.[18–22] In particular, vibrationally-resolved photoelectron spectroscopy[18] indicated that B_{11}^- and B_{11} possess very similar GM structures. Neutral B_{11} cluster was further probed *via* infrared spectroscopy.[19] The GM structures of B_{11}^- and B_{11} were optimized herein at the PBE0/6-311+G* level. The GM structure of B_{11}^- is depicted in Fig. 1; the bond distances are shown in Fig. S1 in the ESI.† It possesses a small vibrational frequency of 148.7 cm^{-1}, which corresponds to the soft mode of in-plane rotation of the peripheral B_9 ring with respect to the inner B_2 dimer. Following this mode, a TS structure was located straightforwardly. The TS also has C_{2v} symmetry (Fig. 1) and one imaginary frequency (143.2*i* cm^{-1}), the latter being related to the in-plane rotation of the peripheral ring. The energy barrier between the GM and TS structures is 0.42 kcal mol^{-1} at PBE0, including zero-point energy (ZPE) corrections. The barrier is further refined to 0.35 kcal mol^{-1} at the single-point CCSD(T) level. This small energy barrier suggests an almost free intramolecular rotation for B_{11}^-. An IRC calculation was carried out at PBE0, ensuring that the TS structure is truly associated with the GM.

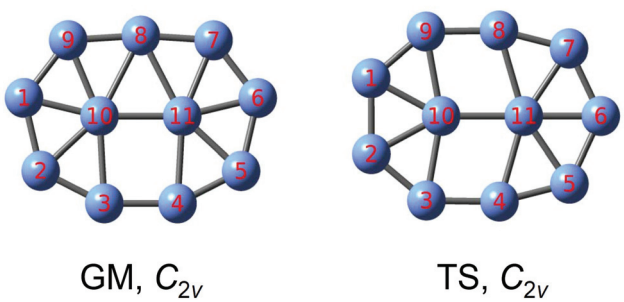

Fig. 1 Optimized structures of the C_{2v} ($^1A_1$) global minimum (GM) and C_{2v} ($^1A_1$) transition state (TS) of B_{11}^- at the PBE0/6-311+G* level.

The soft 148.7 cm^{-1} in-plane rotation of the GM and the corresponding imaginary frequency of 143.2*i* cm^{-1} of the TS are essentially the same vibrational mode, which are associated with a square-to-rhombic conversion of the B3B4B11B10 four-membered hole. The motion in the GM may start with a shrink of the B10B4 distance, which turns the square to a rhombus, the latter corresponding to the bottom rhombic hole in the TS (Fig. 1; right panel). During this motion, the B8B11 distance also shrinks (and the B8B10 distance expands) due to this soft mode, which helps generate a new rhombic B10B9B8B11 hole at the top. This new rhombic hole corresponds to the top hole of the twin in the TS (Fig. 1; right panel). Thus the soft rotational mode easily initiates the motion from the GM to the TS. Interestingly, the B10B4 shrink manages to "push" the B3/B4 atoms to the left, whereas the B8B11 shrink manages to "pull" the B8/B9 atoms to the right. This "push–pull" mechanism provides a driving force for the intramolecular rotation. The above process is reversible *via* a rhombic-to-square conversion associated with a shrink of B3B11 distance and an expansion of B4B10.

Compared to B_{11}^-, the B_{11} neutral cluster has a similar GM structure, C_{2v} ($^2B_2$) (Fig. S2, ESI†), with a soft rotational mode of 153.4 cm^{-1} at PBE0. The intramolecular rotational TS has an imaginary frequency of 165.9*i* cm^{-1} and a slightly higher barrier of 0.55 kcal mol^{-1} at PBE0. At the single-point CCSD(T) level, the rotational barrier is refined to 0.60 kcal mol^{-1}.[30]

To examine the molecular dynamics (MD) behaviors of B_{11}^-, the BOMD simulations were performed at the PBE0/6-31G level, starting from the equilibrium GM geometry with random velocities assigned to the atoms. The initial conditions were chosen to correspond to a microcanonical ensemble (NVE).[31,32] The actual temperature of the system was found to be close to the initial setup during the simulation, for example, 294 K for an initial setup of 300 K. The calculations were done using the Hessian based predictor–corrector method.[33] The Hessian was updated for five steps using Bofill's update method before being recalculated analytically. A step size of 0.5 $amu^{1/2}$ bohr was used for all calculations. The total energy was conserved to 10^{-7} hartree and the total angular momentum was conserved to better than 10^{-8} ħ. Despite the variations of potential and kinetic energies during the BOMD processes, the total energy remains constant in the simulation.

The BOMD results positively confirm the fluxionality of B_{11}^-, at 300, 600, and 900 K. During the simulations, B_{11}^- maintains its planar, elongated geometry and the peripheral ring rotates freely around the B_2 unit, behaving closely like a forwarding tank tread, which is robust and functional even at

900 K. The intramolecular rotation is accomplished by synergistic breaking and making of bonds, which link the peripheral ring and the B_2 core. The inner B_2 bond also breaks occasionally but recovers very quickly. An extracted short movie illustrating the in-plane rotational movements of B_{11}^- during the BOMD simulation, which was performed at 300 K for about 20 ps, is provided in the ESI.† The cluster can accomplish a full turn of rotation approximately in 2 ps. The MD behavior of B_{11} at 300 K is rather similar to that of B_{11}^-, indicating that B_{11} is another molecular tank tread at room temperature.

3.2. A proposed chemical bonding model

To elucidate the intriguing MD behavior of B_{11}^-, it is instructive to start from the analyses of its chemical bonding. A couple of prior papers[18,20–22] have addressed different aspects of the bonding in B_{11}^-. We shall offer here a simple bonding model, as illustrated in Fig. 2.

Basically, we consider the B_{11}^- cluster as the fusion of four rhombic B_4 units: B1B9B8B10, B8B7B6B11, B6B11B4B5, and B1B10B3B2 (Fig. 1). The rhombic B_4 units were lately shown to be the key structural blocks in low-dimensional boron nanostructures.[34,35] As shown in Fig. 2, the bonding between the peripheral B_9 ring and the inner atoms involves both σ and π frameworks. The σ framework is proposed to originate from five two-center two-electron (2c–2e) bonds (Fig. 2; in green). The four rhombic B_4 units each contribute one σ bond along the shorter diagonal, as illustrated in the AdNDP data (Fig. 3a).[21] The inner B_2 also contributes one σ bond (Fig. 3a). This is a zeroth order bonding model.

At different hierarchical levels of approximation, the four diagonal 2c–2e σ bonds readily expand to three- or four-center "islands" (Fig. 3). Ultimately, the global σ framework is completely delocalized, as revealed from the CMOs (Fig. 4b). The π framework is traced to five B centers: B8, B1, B3, B4, and B6, each contributing one electron (Fig. 2; in red). Partial intramolecular electron transfer is discernible in B_{11}^- and B_{11} as revealed from the natural bond orbital (NBO) analysis. This provides the additional π electron, fulfilling the complete, global π sextet.

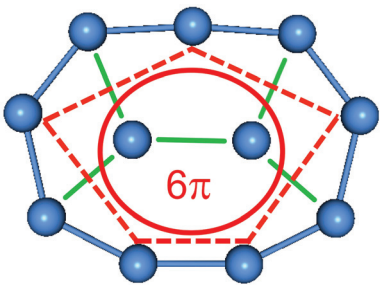

Fig. 2 A zeroth-order bonding model for the B_{11}^- anion. The cluster is proposed to be composed of four B_4 rhombuses around the corners, each contributing one diagonal σ bond for the global σ framework. These in combination with the σ bond in the B_2 core evolve to a delocalized 10σ aromatic system (in green). The remaining five peripheral B centers support an aromatic π sextet (in red), akin to the cyclopentadienyl anion ($C_5H_5^-$).

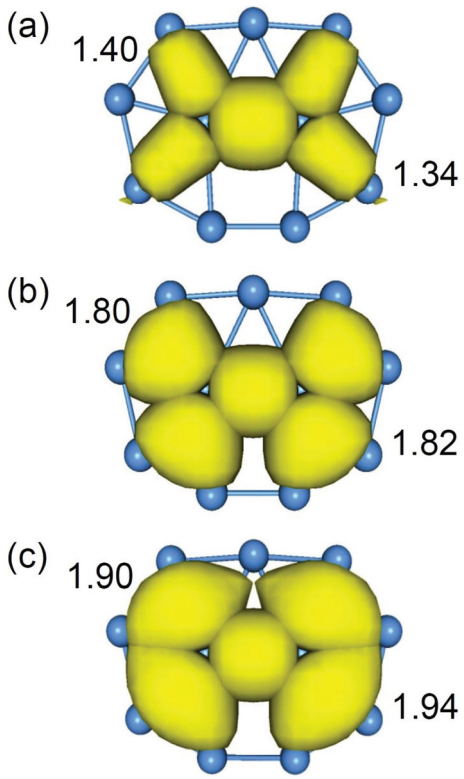

Fig. 3 Different hierarchical levels of approximation for the delocalized σ framework for B_{11}^- as revealed from AdNDP analyses. (a) The 2c–2e presentation of the four diagonal σ bonds and the inner 2c–2e σ bond. (b) The 3c–2e presentation of the diagonal σ bonds. (c) The 4c–2e presentation of the diagonal σ bonds. Occupation numbers (ONs) are indicated, showing that the 3c–2e presentation is sufficiently accurate for the diagonal σ bonds.

The π sextet in B_{11}^- (Fig. 2) is reminiscent of the aromatic cyclopentadienyl anion ($C_5H_5^-$), hinting that B_{11}^- is an all-boron analogue of $C_5H_5^-$. Zhai *et al.*[18] first suggested this interesting analogy, primarily on the basis that both species are aromatic anions with 6π electrons. However, it was unclear previously how the two systems are structurally connected, how an 11-center B cluster becomes analogous to a 5-center C based system, and where the π electrons originate exactly. The present bonding model (Fig. 2) fully addresses all these questions. Moreover, the simple model allows an in-depth mechanistic understanding of the dynamic properties of B_{11}^- and B_{11} as subnanoscale tank treads.

This bonding model is basically, but not explicitly, in the spirit of the classical Lewis description. It makes full use of the three valence electrons for each B atom in the electron-deficient cluster. In essence, B_{11}^- is a doubly (π and σ) aromatic system with 6π and 10σ electrons (Fig. 4), each conforming to the $(4n + 2)$ Hückel rule. In addition, the peripheral B_9 ring is linked by nine 2c–2e σ bonds, which are perfectly recovered in the AdNDP data (Fig. 5b), as well as revealed from the CMO analysis (Fig. 4a).

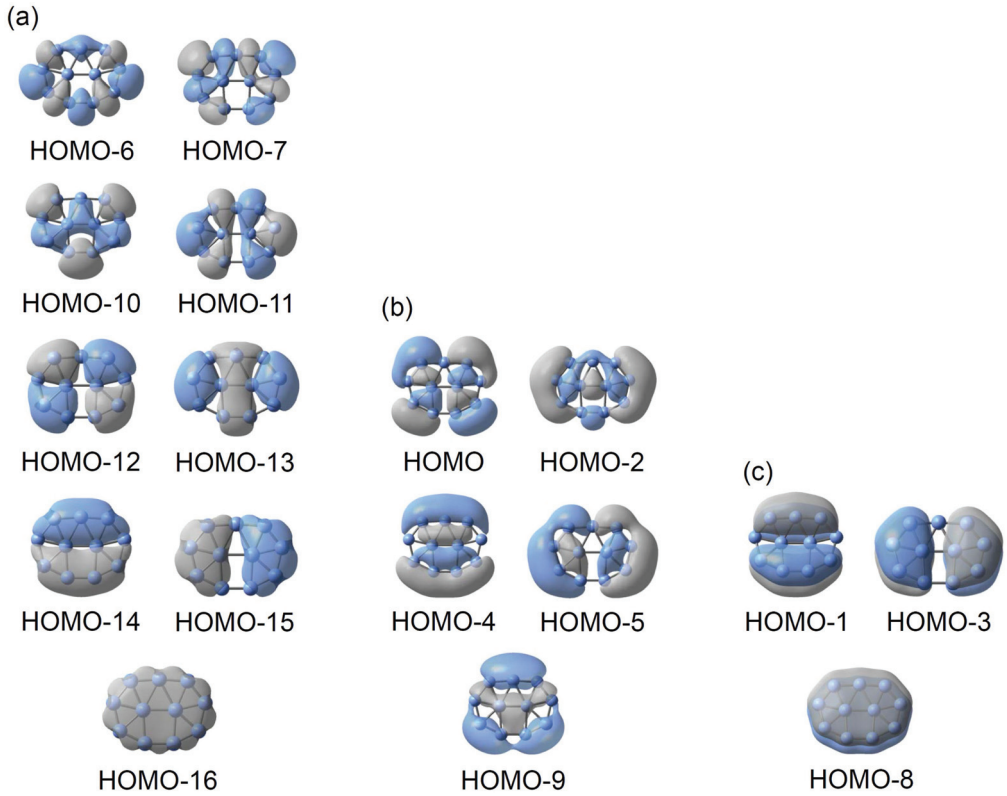

Fig. 4 Cannonical molecular orbitals of the C_{2v} ($^1A_1$) global minimum of B_{11}^-. (a) The set of nine peripheral σ bonds, which are readily localized as 2c–2e σ bonds. (b) Five globally delocalized σ bonds. (c) Three globally delocalized π bonds. The delocalized π and σ bonds show one-to-one correspondence to each other. The 6π and 10σ electrons in (b) and (c) conform to the (4*n* + 2) Hückel rule for aromaticity. The "island" AdNDP patterns in Fig. 3 are only an approximate, localized view of a truly delocalized σ system.

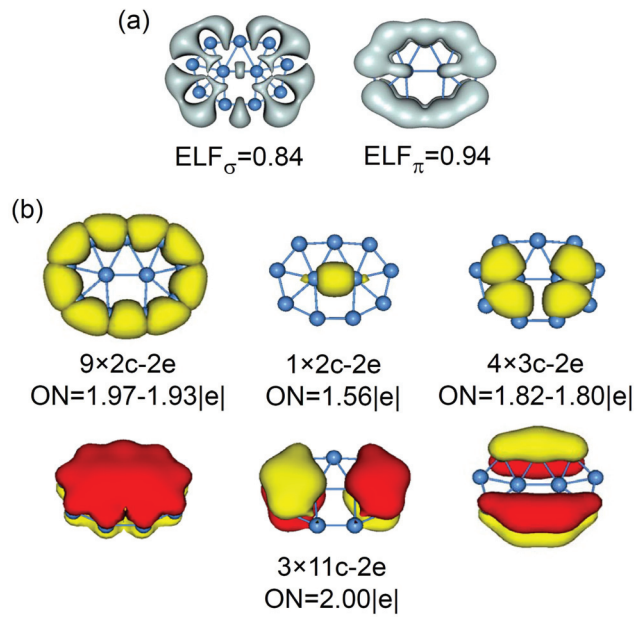

Fig. 5 Chemical bonding in the C_{2v} ($^1A_1$) global minimum of B_{11}^-. (a) Electron localization functions (ELFs); the total ELF is shown in Fig. S3 in the ESI.† (b) Bonding elements as revealed using the AdNDP, along with the occupation numbers (ONs).

3.3. The three-center island version: a sufficient description of the σ bonding in the global minimum

For the mechanistic understanding of B_{11}^- as a tank tread, we choose to use the three-center island version for the four diagonal σ bonds (Fig. 3b and 5b), which originates from the diagonal 2c–2e σ bonds (Fig. 2; in green). Considering the fact that each B atom in the B_2 core is hexacoordinated, the occupation number (ON) of 1.56|*e*| in AdNDP, which is equivalent to a bond order of around 0.8, indicates a reasonably well-defined σ bond. This is fully supported by the ELF analysis, which shows no evidence of multicenter delocalization for this bond (Fig. 5a; Fig. S3, ESI†). Manual expansion of the core 2c–2e σ bond to 3c–2e (B10B11B8) or even 5c–2e (B10B8B11B4B3) does not improve our understanding of the bonding in the system, because the electron cloud in the 3c–2e or 5c–2e option is overwhelmingly dominated by the B10B11 core (~80%).

Additional arguments for the validity of the core 2c–2e σ bond approximation include: (i) the hypercoordinated core is the most electron-deficient portion in the system, and it can never have an ON that is even close to ideal. Note that for example, a report shows lately that the ON for certain bonds in the B_{30}^- cluster amounts to 1.6|*e*| (even for 4c–2e bonds).[36] (ii) A very recent study using the orbital localization procedure

based on the ELF (ELF-LOC) results in an ON of 1.99|*e*| for this bond, which provides further support for the nature of the 2c–2e bond in the core.[37] (iii) If this σ bond were indeed 3c–2e or 5c–2e in nature (that is, the additional B centers make significant contributions), then its ON should change markedly from the GM to the TS, where in the latter the coordination environment of the B_2 core alters; this is not the case: ON = 1.56|*e*| in GM (Fig. 5b) *versus* ON = 1.57|*e*| in the TS (Fig. S4, ESI†). (iv) The MD simulations show that the B10–B11 link is the most robust of all links that are associated with the central B atoms, whereas the B8B10 or B8B11 link in the B8B10B11 triangle is among those susceptible to breakage. This dynamic behaviour is also in line with the 2c–2e picture.

For the four diagonal 2c–2e σ bonds, the ONs amount to 1.34 and 1.40|*e*| (Fig. 3a) and are far less than ideal. Expanding these bonds to three-center delocalization (Fig. 3b) substantially enhances the ONs to 1.82 and 1.80|*e*|, respectively. However, further expansion to 4c–2e bonds helps very little. The fourth B atom contributes negligibly, that is, only 25% of the third B atom (Fig. 3c). On the basis of the evolution of ONs, it may be stated that the 2c–2e description for the diagonal σ bonds captures 70% of the essence, whereas the four 3c–2e σ bonds recover that by 90%. The latter bonding picture is sufficiently accurate, in particular considering that it represents a localized view (Fig. 3b) of an aromatic 10σ system (Fig. 4b).

3.4. Structural evolution during the intramolecular rotation

Fig. 6 shows how the structure of B_{11}^- changes along the rotational coordinate in the MD process (and a similar illustration for the B_{11} neutral is shown in Fig. S5, ESI†). Assume that the cluster rotates clockwise. At the initial GM_1 structure, the B3 and B4 atoms are located at the bottom of the square hole, which appears to be the most flexible part in the GM. As the square hole tilts toward the left, the whole B_9 ring adjusts spatially around the B_2 core, leading to the $TS_{1\text{-}2}$ structure, whose C_2 axis is perpendicular to that of GM_1. Note that two tilted four-membered rings are present in $TS_{1\text{-}2}$. Passing the barrier, the top four-membered ring turns square, reaching the GM_2 structure, which is effectively GM_1 with a 180° in-plane rotation. From GM_1 to GM_2, the B4 atom moves by half a link, as does every other peripheral B atom. The evolution from GM_2 to GM_3 *via* $TS_{2\text{-}3}$ is similar to that from GM_1 to GM_2, allowing the B4 atom to move half a link further to the left. Overall, from GM_1 to GM_3 every peripheral atom shifts clockwise by one link (or by 40° in average), the tank tread moves one link to the right, and the GM structure recovers its initial geometry and orientation. In the process, the C_2 axis rotates four times, each time by 90°. By repeating the above process 9 times, the tank tread moves a whole turn and every B atom recovers its exact initial position.

To reconcile the established high stability[18] of B_{11}^- (the HOMO–LUMO gap calculated in the current work is 3.00 eV at the PBE0/6-311+G* level) with its fluxionality, we emphasize two factors: electron-deficiency and structural defect. The former results in a greatly reduced number of available bonds between the peripheral ring and the core (Fig. 2), whose delocalization further facilitates their use as "lubricant" for the intramolecular rotation (Fig. 3). The square hole in the GM (Fig. 1) may be viewed as a structural defect for a triangular close-packing planar system. This flexible defect can initiate the in-plane rotation *via* the soft vibrational mode, with little extra energy.

3.5. Electron shift and flow during the intramolecular rotation

The fluxionality of B_{11}^- and B_{11} may be attributed to their unique bonding. The peripheral B_9 ring is connected by 2c–2e σ bonds, as is the inner B_2 dimer. However, the bonding

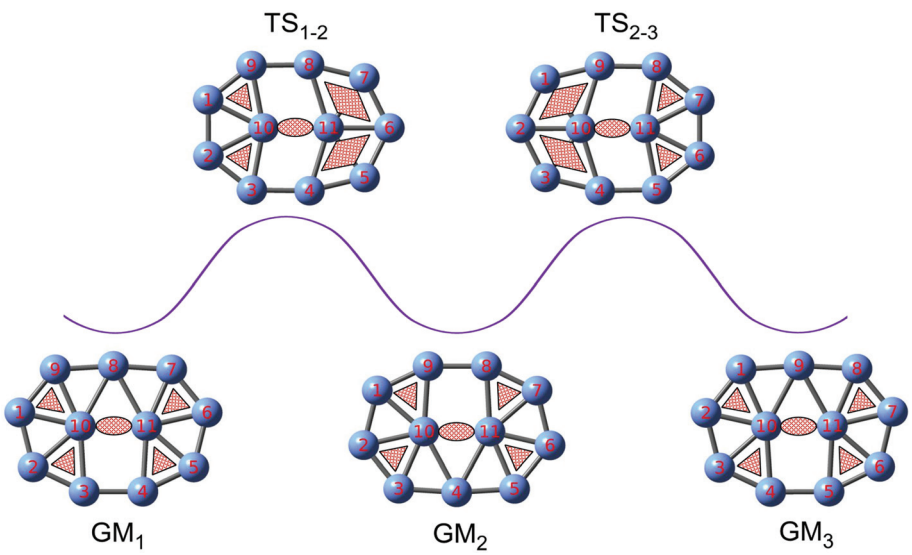

Fig. 6 The evolution of the structure and delocalized diagonal σ bonds (shaded triangles and diamonds; in red) during the peripheral rotation of the B_{11}^- cluster.

between the inner and peripheral portions is electron-deficient and entirely delocalized. While as many as 10 such BB "bonds" are illustrated in the GM structure of B_{11}^- and 9 "bonds" in the TS (Fig. 1), none of these is a real bond. Even the four diagonal σ bonds (Fig. 2) are only a zeroth order approximation. In fact, the peripheral ring and the B_2 core are connected by completely delocalized σ and π clouds (five σ bonds *versus* three π bonds; Fig. 4).

In the MD process, each rhombic B_4 unit is flexible, whose adjustment in shape sensitively affects the spatial distribution of the island σ cloud (Fig. 6). Take the B1B9B10 triangle as an example. At the initial GM_1 and at $TS_{1\text{-}2}$ as well, the σ cloud is islanded on this triangle and leans to the B9B10 edge. At GM_2 the σ cloud remains in the B1B9B10 triangle, but the density now shifts to the B1B10 edge. Upon further rotation of the peripheral ring, the σ cloud gradually extends to the whole rhombus of B2B1B9B10 at $TS_{2\text{-}3}$. Passing the barrier of $TS_{2\text{-}3}$, the rhombic σ cloud shrinks and condenses at GM_3 to the other end of B2B1B9B10, that is, the B2B1B10 triangle (and remains leaning to the B1B10 edge). This completes the cycle: the cluster returns to the initial GM position, as is the σ cloud; and yet the peripheral B atom moves one link and the σ cloud shifts by one triangle. In other words, the island electron cloud flows and shifts continuously like a liquid in the rhombus during the MD process, which reinforces the structural rearrangement; and *vice versa*. This motion process requires little extra energy in each step, consistent with the small rotational barrier.

It is stressed that, in the TS structure, the four-center delocalization of the island σ cloud, as compared to the three-center case in the GM, is genuine (Fig. 3b *versus* Fig. 7c). AdNDP analysis for the TS of B_{11}^- shows that in the B4B11B6B5 rhombus the contribution of the fourth atom, B4, to the ON is about 60% of the third one, B6, and thus none should be ignored (Fig. 7c). Interestingly, the flow and shift of island σ cloud counter the rotational direction of the peripheral ring (Fig. 6), which manages to maintain the four island σ bonds at roughly the same positions of the cluster, despite the rotation of the atoms.

One may argue that the 2c–2e B–B σ bond in the core has a low ON (Fig. 5b); we have reasoned carefully in Section 3.3 that this ON value is reasonable. Note that this bond can be manually expanded to 3c–2e (B10B11B8) or even 5c–2e (B10B8B11B4B3), but in such an expanded σ bond, the electron cloud is still dominated by the B10B11 core (~80%). The "dilute" electron cloud on the additional B8/B4/B3 centers is not anticipated to have a negative impact on the in-plane rotation of the subnanoscale tank tread.

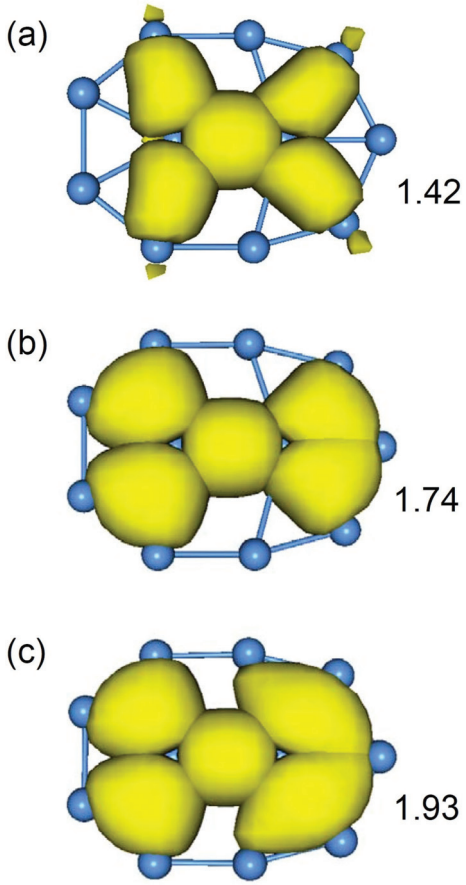

Fig. 7 AdNDP analyses for the delocalized σ framework in the C_{2v} transition state of the B_{11}^- anion. (a) 2c–2e presentation of the four diagonal σ bonds and the inner 2c–2e σ bond. (b) 3c–2e presentation of the diagonal σ bonds. (c) 3c–2e plus 4c–2e presentation of the diagonal σ bonds, where the two σ bonds at the right side are four-center in nature. Occupation numbers (ONs) are indicated.

4. Conclusions

Continuous tracks dated back as early as the 1770s. Tanks as armoured fighting vehicles were first used during World War I. However, no one seemed to have imagined of the miniaturization of a tank tread down to the sub-nanometer scale. Even with the very recent discoveries of boron molecular wheels and Wankel motors, the free in-plane rotation of the elongated all-boron clusters such as B_{11}^- and B_{11} has not been speculated or tested. Indeed, the inner B_2 dimer may be intuitively viewed as a bar that halts the intramolecular rotation. The current finding is thus beyond imagination. It is remarkable that a self-assembly of as few as eleven boron atoms can function basically as a subnanoscale tank tread, whose macroscopic counterpart is rather sophisticated. It may be argued that B_{11}^- and B_{11} serve not only as molecular tank treads, but also as molecular motors at the room temperature and beyond. We expect that the B_{11}^-/B_{11} tank treads will inspire scientists to search for and design more novel boron nanostructures and to fabricate boron-based nanomachines, such as a nanotank. Not surprisingly, the clockwise or anticlockwise rotation of the tank tread is completely random. Nonetheless, it should be possible to control the unidirectional rotation[15] using a strategy similar to that proposed for a Wankel motor. On a properly engineered, inert surface, the molecular tank treads may maintain their structural, electronic, and dynamic integrity.

Acknowledgements

This work was supported by the National Natural Science Foundation of China (21243004, 21373130, and 21573138) and the State Key Laboratory of Quantum Optics and Quantum Optics Devices (KF201402). H.J.Z. gratefully acknowledges the start-up fund from Shanxi University for support.

References

1 C. Joachim and G. Rapenne, *ACS Nano*, 2013, **7**, 11.
2 K. E. Drexler, *Nanosystems: Molecular Machinery, Manufacturing, and Computation*, John Wiley & Sons, Inc., New York, USA, 1992.
3 R. E. Smalley, *Sci. Am.*, 2001, **285**, 76.
4 A. Ricca and C. W. Bauschlicher, *Chem. Phys.*, 1996, **208**, 233.
5 I. Boustani, *Phys. Rev. B: Condens. Matter*, 1997, **55**, 16426.
6 J. E. Fowler and J. M. Ugalde, *J. Phys. Chem. A*, 2000, **104**, 397.
7 J. I. Aihara, H. Kanno and T. Ishida, *J. Am. Chem. Soc.*, 2005, **127**, 13324.
8 E. Oger, N. R. M. Crawford, R. Kelting, P. Weis, M. M. Kappes and R. Ahrichs, *Angew. Chem., Int. Ed.*, 2007, **46**, 8503.
9 H. J. Zhai, Y. F. Zhao, W. L. Li, Q. Chen, H. Bai, H. S. Hu, Z. A. Piazza, W. J. Tian, H. G. Lu, Y. B. Wu, Y. W. Mu, G. F. Wei, Z. P. Liu, J. Li, S. D. Li and L. S. Wang, *Nat. Chem.*, 2014, **6**, 727.
10 H. J. Zhai, A. N. Alexandrova, K. A. Birch, A. I. Boldyrev and L. S. Wang, *Angew. Chem., Int. Ed.*, 2003, **42**, 6004.
11 W. Huang, A. P. Sergeeva, H. J. Zhai, B. B. Averkiev, L. S. Wang and A. I. Boldyrev, *Nat. Chem.*, 2010, **2**, 202.
12 J. O. C. Jiménez-Halla, R. Islas, T. Heine and G. Merino, *Angew. Chem., Int. Ed.*, 2010, **49**, 5668.
13 F. Cervantes-Navarro, G. Martínez-Guajardo, E. Osorio, D. Moreno, W. Tiznado, R. Islas, K. J. Donald and G. Merino, *Chem. Commun.*, 2014, **50**, 10680.
14 G. Martínez-Guajardo, A. P. Sergeeva, A. I. Boldyrev, T. Heine, J. M. Ugalde and G. Merino, *Chem. Commun.*, 2011, **47**, 6242.
15 J. Zhang, A. P. Sergeeva, M. Sparta and A. N. Alexandrova, *Angew. Chem., Int. Ed.*, 2012, **51**, 8512.
16 D. Moreno, S. Pan, L. L. Zeonjuk, R. Islas, E. Osorio, G. Martínez-Guajardo, P. K. Chattaraj, T. Heine and G. Merino, *Chem. Commun.*, 2014, **50**, 8140.
17 A. D. Zdetsis, *J. Chem. Phys.*, 2007, **127**, 014314.
18 H. J. Zhai, B. Kiran, J. Li and L. S. Wang, *Nat. Mater.*, 2003, **2**, 827.
19 C. Romanescu, D. J. Harding, A. Fielicke and L. S. Wang, *J. Chem. Phys.*, 2012, **137**, 014317.
20 D. Yu. Zubarev and A. I. Boldyrev, *J. Comput. Chem.*, 2007, **28**, 251.
21 D. Yu. Zubarev and A. I. Boldyrev, *Phys. Chem. Chem. Phys.*, 2008, **10**, 5207.
22 T. B. Tai, D. J. Grant, M. T. Nguyen and D. A. Dixon, *J. Phys. Chem. A*, 2010, **114**, 994.
23 C. Adamo and V. Barone, *J. Chem. Phys.*, 1999, **110**, 6158.
24 R. Krishnan, J. S. Binkley, R. Seeger and J. A. Pople, *J. Chem. Phys.*, 1980, **72**, 650.
25 M. J. Frisch, *et al.*, *Gaussian 09, revision A.2*, Gaussian Inc., Wallingford, Connecticut, 2009.
26 G. D. Purvis and R. J. Bartlett, *J. Chem. Phys.*, 1982, **76**, 1910.
27 B. Silvi and A. Savin, *Nature*, 1994, **371**, 683.
28 AdNDP is an extension of the natural bond orbital (NBO) analysis. AdNDP represents the bonding of a molecule in terms of *n*-center two-electron (*n*c–2e) bonds, with *n* ranging from one to the total number of atoms in the system. AdNDP analysis thus recovers not only the classical Lewis bonding elements (lone pairs and 2c–2e bonds), but also the delocalized *n*c–2e bonds.
29 U. Varetto, *Molekel 5.4.0.8*, Swiss National Supercomputing Center, Manno, Switzerland, 2009.
30 The structural, electronic, and bonding properties of B_{11} are very similar to those of B_{11}^-, except that they differ by one valence electron.
31 X. S. Li, J. M. Millam and H. B. Schlegel, *J. Chem. Phys.*, 2001, **114**, 8897.
32 X. S. Li, J. M. Millam and H. B. Schlegel, *J. Chem. Phys.*, 2001, **115**, 6907.
33 J. M. Millam, V. Bakken, W. Chen, W. L. Hase and H. B. Schlegel, *J. Chem. Phys.*, 1999, **111**, 3800.
34 H. J. Zhai, Q. Chen, H. Bai, H. G. Lu, W. L. Li, S. D. Li and L. S. Wang, *J. Chem. Phys.*, 2013, **139**, 174301.
35 H. J. Zhai, Q. Chen, H. Bai, S. D. Li and L. S. Wang, *Acc. Chem. Res.*, 2014, **47**, 2435.
36 W. L. Li, Y. F. Zhao, H. S. Hu, J. Li and L. S. Wang, *Angew. Chem., Int. Ed.*, 2014, **53**, 5540.
37 O. B. Ona, J. J. Torres-Vega, A. Torre, L. Lain, D. R. Alcoba, A. Vasquez-Espinal and W. Tiznado, *Theor. Chem. Acc.*, 2015, **134**, 28.

